



## Small angle X-ray scattering measurements of spatial dependent linewidth in dense nanoline gratings<sup>☆</sup>

Chengqing Wang<sup>a</sup>, Wei-En Fu<sup>b</sup>, Bin Li<sup>c</sup>, Huai Huang<sup>c</sup>, Christopher Soles<sup>a</sup>, Eric K. Lin<sup>a</sup>, Wen-li Wu<sup>a,\*</sup>, Paul S. Ho<sup>c</sup>, Michael W. Cresswell<sup>d</sup>

<sup>a</sup> Polymers Division, National Institute of Standards and Technology, Gaithersburg, MD 20899-8541, United States

<sup>b</sup> Center for Measurement Standards, Industrial Technology Research Institute, Hsinchu, 300, Taiwan

<sup>c</sup> Microelectronics Research Center, The University of Texas at Austin, 10100 Burnet Road, Bldg 160, Austin, TX 78758, United States

<sup>d</sup> Semiconductor Electronics Division, National Institute of Standards and Technology, Gaithersburg, MD 20899-8120, United States

### ARTICLE INFO

#### Article history:

Received 21 August 2008

Received in revised form 5 March 2009

Accepted 6 March 2009

Available online 16 March 2009

#### Keywords:

Small angle X-ray scattering

Electron beam lithography

Anisotropic wet etching

Linewidth

Silicon wafer

Line gratings

### ABSTRACT

Small angle X-ray scattering (SAXS) was used to characterize the cross section of nanoline gratings fabricated with electron beam lithography (EBL) patterning followed by anisotropic wet etching into a single crystal silicon substrate. SAXS results at normal incidence clearly bear the signature of positional dependent linewidth within the gratings; such non-uniformity is subsequently confirmed with scanning electron microscopy. The proximity effect of EBL is believed to be the cause of the spatial variations of linewidth. To quantitatively fit the SAXS results the linewidth near the periphery of the patterned field needs to be 80% greater than that in the central region, whereas the cross section of nanolines can be modeled as a simple rectangular shape, as expected from the anisotropic wet etching process.

Published by Elsevier B.V.

As the minimum feature size in integrated circuits approaches 32 nm and smaller, significant challenges arise in quantifying both the statistically averaged feature dimension as well as variations from the average. Scanning electron microscopy (SEM), optical scatterometry and atomic force microscopy are approaching their sensitivity limits at this size scale [1] especially for patterns with dense and high aspect ratio features. In this work, we illustrate the use of an X-ray based method to quantify densely packed nanolines with an aspect ratio approaching 20. There is a clear need to have a reference metrology that can provide reliable and accurate reference data for benchmarking and calibration purposes. Transmission small angle X-ray scattering (SAXS) is an emerging dimensional metrology platform to provide quantitative data on pitch, linewidth, line height, sidewall angle and line edge roughness with sub-nm precision [2–5]. Besides transmission SAXS, grazing incidence small angle X-ray scattering (GISAXS) has also been applied to measure periodic nanostructures [6–10], including one dimensional gratings and two dimension island arrays. In comparison, the quantitative analysis of transmission SAXS data can be conducted via the classical kinematic scattering theory whereas the complicated dynamic theory with various approximations becomes necessary for GISAXS data analysis.

For cross calibration purposes, it is desirable to have robust and stable test samples that can be used in SAXS as well as other well established metrologies, including SEM. Line/space gratings with sub-50 nm dense silicon lines on silicon wafers can serve this purpose [11]. In this study we use a top-down fabrication process that combines EBL and anisotropic wet etching to obtain single crystal dense line/space gratings. It is well known that EBL is capable of generating sub-20 nm features via high resolution e-beam resists and anisotropic wet etching can transfer the features onto silicon wafers with nearly atomically flat sidewalls due to the grossly different dissolution rates on different crystalline planes [12]. A three dimensional schematic of a line grating created with a wet etching process is given in Fig. 1. The details of the EBL and the wet etching process can be found elsewhere [13].

SAXS data were collected at the 5-ID-DND beamline of the Advanced Photon Source at Argonne National Laboratory. The data were collected in transmission through the silicon substrate using a 17 keV X-ray beam with a corresponding wavelength ( $\lambda_x$ ) of  $(0.0729 \pm 0.0003)$  nm [14]. The scattered X-rays were collected on a two-dimensional CCD detector with a sample-to-detector distance of  $(719.3 \pm 0.5)$  cm. As illustrated in the inset of Fig. 2, X-ray data were collected as a function of the sample rotation angle,  $\omega$ , over a range of  $-30^\circ$  to  $+30^\circ$  in  $0.5^\circ$  increments, where  $\omega = 0^\circ$  is defined as the condition where the incident X-ray beam is normal to the substrate, i.e., along the z-axis defined in Fig. 1. The rotation axis is parallel to that of the lines in the patterns and is designated as the y-axis in Fig. 1.

<sup>☆</sup> Official contribution of the National Institute of Standards and Technology; not subject to copyright in the United States.

\* Corresponding author.

E-mail address: [wenli@nist.gov](mailto:wenli@nist.gov) (W. Wu).

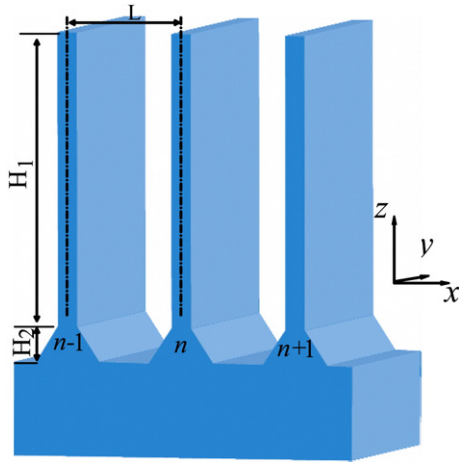


**Fig. 1.** A three-dimensional illustration of the nanolines on (110) silicon wafer. The cross section of the nanolines consists of two parts – a rectangle top and a trapezoid base.

The sector average of the 2-D data along the diffraction axis ( $x$ -axis) provided  $I(q)$  at each rotation angle, and a compilation of  $I(q)$  at all the rotation angles generated a data set  $I(q, \omega)$ , where  $q = 4\pi/\lambda_x \sin(\theta)$  and  $2\theta$  is the scattering angle. The data were then converted to  $I(q_x, q_z)$  using a standard rotation matrix scheme [2].

The nanoline cross section is modeled with a top part closely resembling a rectangle and a trapezoid bottom part. The corresponding cross section in Fourier space, i.e., the form factor of  $n$ th nanoline, can be expressed as

$$f_n(q_x, q_z) = f_{\text{top}}(q_x, q_z) + f_{\text{bottom}}(q_x, q_z). \tag{1}$$

The form factor of the whole nanoline grating is simply

$$F(q_x, q_z) = \sum_n f_n(q_x, q_z) \exp(-iq_x nL), \tag{2}$$

where  $L$  is the pitch. The experimental SAXS data from our test grating is given in Fig. 2 and the data qualitatively suggests vertical sidewalls [3]. To quantitatively fit the experimental data, the top part is modeled as an asymmetrical trapezoid with two sidewall slopes  $k_1$  and  $k_2$ , and the bottom part is modeled as a trapezoid with its sidewall angle fixed at  $35.3^\circ$ , which is the angle between (111) and (100) silicon planes. Because the sidewall angle of the bottom part is very large, the corresponding SAXS signal resides outside the experimental data range, hence, it is not included in the fitting parameters. A weighted

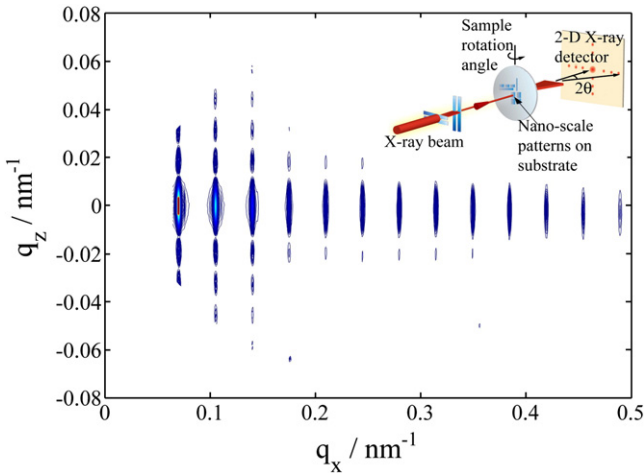


**Fig. 2.** Experimental X-ray scattering intensities on the  $q_x$ – $q_z$  plane from the test gratings. The configuration used in our transmission SAXS measurements is given as the inset.

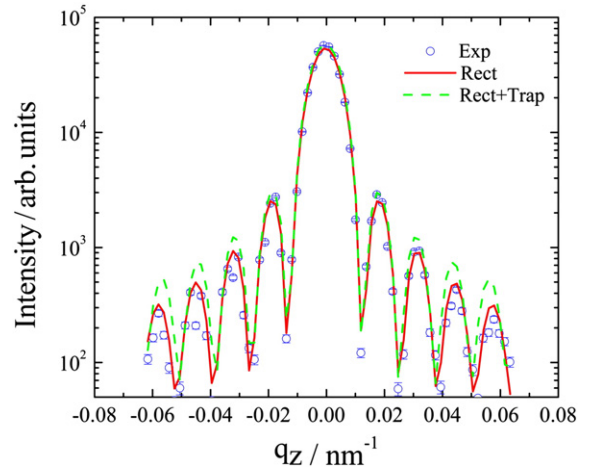


**Fig. 3.** Experimental scattering intensities as a function of  $q_z$  at  $q_x = 0.105 \text{ nm}^{-1}$  (blue circle) in comparison with two model calculations. Shown are model fitting with a rectangle cross section alone (red solid line) and with a rectangle top plus a trapezoid bottom (green dash line) where the bottom height was fixed at 50 nm.

nonlinear least squares fitting algorithm was used to determine all the dimensional parameters including  $k_1$  and  $k_2$ . As the first step we estimated the contribution to the observed scattering intensity from the bottom trapezoid as follows. Fig. 3 provides the scattering intensity vs.  $q_z$  along a constant value of  $q_x$  at  $0.105 \text{ nm}^{-1}$  which corresponds to the second lowest order of diffraction peaks along  $q_z = 0$ . This second order diffraction peak is chosen in lieu of the first one simply because data over a wide range of  $q_z$  are available at this  $q_x$ . To our surprise, a simple rectangular cross section with a vertical sidewall and a height ( $H_1$ ) of  $(489.5 \pm 5) \text{ nm}$  fits the experimental data well even without the bottom trapezoid. A quantitative fit of the experimental data with a model composed of a rectangular top and a trapezoidal bottom results in the height of the trapezoidal bottom part being close to zero. To accentuate this point, when we forced the bottom trapezoid to have a 50 nm height and let the height of the top rectangle vary, the fit between the model and experimental data deteriorated noticeably, especially in high  $q_z$  region (Fig. 3). This suggests that the bottom trapezoid can be neglected to fit the data given in Fig. 2. Without the bottom trapezoid, a further fit indicates that the sidewall angles of the top trapezoid are smaller than  $0.1^\circ$ , which is within the experimental uncertainty! Thus the sidewalls of the top part are essentially vertical. In others words, a simple

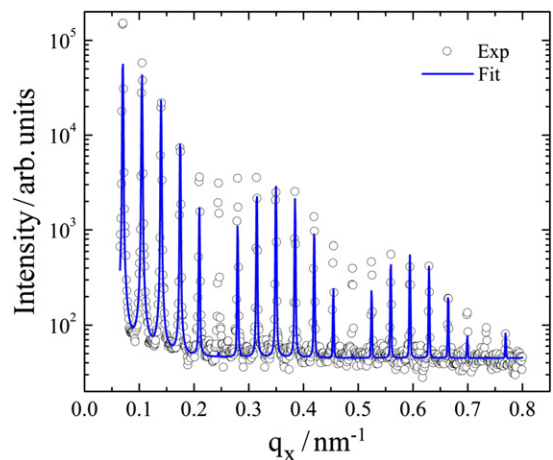


**Fig. 4.** Experimental scattering intensities as a function of  $q_x$  at  $q_z = 0$  (open circle) and the best fit with nanolines with a rectangular cross section and a uniform linewidth.

rectangular cross section is sufficient to fit the nanolines and will be used for discussions in the rest of this work.

Discrepancies between the model fitting using the rectangular cross section of uniform linewidth and the experimental data in Fig. 2 are evident near  $q_x$  values of  $0.25 \text{ nm}^{-1}$  and  $0.5 \text{ nm}^{-1}$ . The experimental data shows significant intensities near these two regions along all the  $q_z$  whereas the model fit yields near zero intensity. To further examine this discrepancy we first focus our efforts on the data at  $q_z=0$ , i.e. data collected with normal incident beam. Experimental data at  $q_z=0$  and the best fit using a rectangular cross section of a uniform linewidth of  $26.9 \text{ nm}$  are given in Fig. 4, and the above mentioned discrepancy between the data and the fit at  $q_x \approx 0.25 \text{ nm}^{-1}$  and  $q_x \approx 0.5 \text{ nm}^{-1}$  is clearly noticeable. The peak intensity envelope of the experimental data seems to be smeared out in these two regions.

In searching for the cause of this smearing out effect, we conducted high resolution SEM measurements of the nanoline gratings using a Hitachi S-4700 equipped with a field emission electron gun [15]. A scan along the direction perpendicular to the grating trenches from the one edge of patterned field to the opposite edge shows that the linewidths are far from being uniform. The nanolines within approximately  $10 \mu\text{m}$  of the pattern edge are nearly twice as wide as those in the center part of the pattern. In addition, the line edge roughness of nanolines near the patterned edge is much larger than that of those in the center. A summary of the SEM results on linewidth is given in Fig. 5. This observed variation in linewidth between edges and the center of the patterned field is consistent with the well-known EBL proximity effect. During the EBL exposure, the back scattered electrons from the substrate contribute significantly to the total e-beam dosage; the area in the central region of a patterned field receives higher total dosages than the border region. For the type of photoresist used in this work high exposure dosage leads to thin lines. In our sample preparation, no exposure corrections were attempted in the EPL process to counter the proximity effect. We did not mask off the border region before the chemical etching process either. It is therefore not a surprise that there exists such a large variation in linewidth within a grating.

In the following data fitting we model the local linewidth  $w_n$  at the  $n$ th line by a simple function  $\{w_0^* (1 + 1.8 | \frac{n}{N} - \frac{1}{2} |)^3\}$  where  $w_0$  is the linewidth of the central line and  $N$  is total number of lines. Fig. 6 shows a weighted nonlinear least squares fitting of diffraction intensity using the above linewidth distribution function. This fitting now successfully captures the smearing effects of scattering intensities near  $0.25 \text{ nm}^{-1}$  and  $0.5 \text{ nm}^{-1}$  and it results in an average linewidth of  $w_0 = (24.9 \pm 0.5) \text{ nm}$  at the pattern center and a pitch of  $(180.1 \pm 0.2) \text{ nm}$ . This value of  $w_0$  is consistent with the SEM results

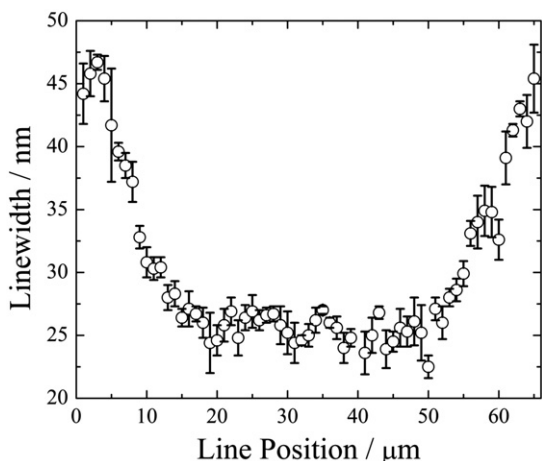


Fig. 5. Linewidth measured with top-down SEM. A strong dependence of linewidth on its position is evident.

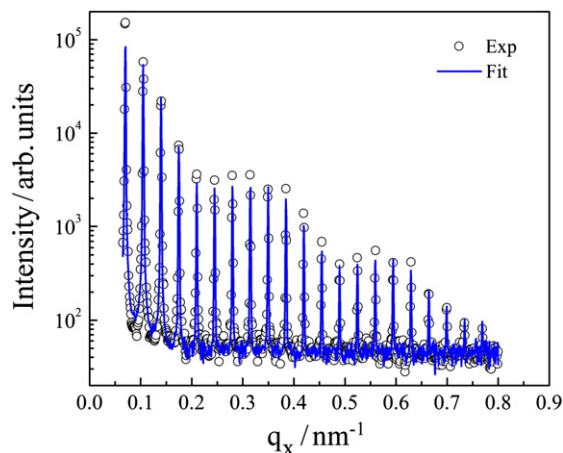


Fig. 6. Experimental scattering intensity as a function of  $q_x$  at  $q_z=0$  (open circle) and the best fit with nanolines with a rectangular cross section and a non-uniform linewidth.

given in Fig. 5. As discussed earlier, the height of the nanolines was determined to be  $489.5 \text{ nm}$  by fitting the data along  $q_z$ , and this renders an aspect ratio as high as  $19.7$  for the nanolines near the center of the pattern. In general, we believe that nanopatterns with high aspect ratios can be readily characterized using SAXS due to the penetration power of X-rays. We expect that other high aspect ratio structures including poles and deep vias can all be characterized by this X-ray technique.

In summary, we demonstrate the use of transmission SAXS to characterize the cross section of single crystal silicon nanolines fabricated through a combination of electron beam lithography and an anisotropic wet etching processes. The cross section of each nanoline was accurately modeled as a rectangular with vertical sidewalls, consistent with the anisotropic dissolution kinetics along different crystallographic planes. The dense line/space gratings have a U-shaped linewidth distribution which is believed to be caused by the proximity effect during the EBL process. The non-uniformity in linewidth can be readily detected and quantitatively analyzed from the experimental data collected under a simple normal incident geometry.

#### Acknowledgement

This work was funded in part by the NIST Office of Microelectronics Program. Use of the Advanced Photon Source was supported by the U.S. Department of Energy, Office of Science, Office of Basic Energy Sciences, under Contract No. DE-AC02-06H11357. The authors are grateful to Mr. Kwang-Woo Choi of Intel for his assistance in SEM measurements.

#### References

- [1] International Technology Roadmap for Semiconductors, Metrology, 2007 <http://www.itrs.net/Links/2007ITRS/Home2007.htm>.
- [2] R.L. Jones, T. Hu, E.K. Lin, W.L. Wu, R. Kolb, D.M. Casa, P.J. Bolton, G.G. Barclay, Appl. Phys. Lett. 83/19 (2003) 4059.
- [3] T.J. Hu, R.L. Jones, W.L. Wu, E.K. Lin, Q.H. Lin, D. Keane, S. Weigand, J. Quintana, J. Appl. Phys. 96/4 (2004) 1983.
- [4] C.Q. Wang, R.L. Jones, E.K. Lin, W.L. Wu, J. Leu, Appl. Phys. Lett. 90/19 (2007) 193122.
- [5] C.Q. Wang, R.L. Jones, E.K. Lin, W.L. Wu, B.J. Rice, K.W. Choi, G. Thompson, S.J. Weigand, D.T. Keane, J. Appl. Phys. 102/2 (2007) 024901.
- [6] M. Tolan, G. König, L. Brugemann, W. Press, F. Brinkop, J.P. Kotthaus, Europhys. Lett. 20/3 (1992) 223.
- [7] T.H. Metzger, K. HajYahya, J. Peisl, M. Wendel, H. Lorenz, J.P. Kotthaus, G.S. Cargill, J. Appl. Phys. 81/3 (1997) 1212.
- [8] M. Yan, A. Gibaud, J. Appl. Crystallogr. 40 (2007) 1050.
- [9] Q. Shen, C.C. Umbach, B. Weselak, J.M. Blakely, Phys. Rev. B 48/24 (1993) 17967.
- [10] T. Baumbach, D. Lubbert, J. Phys., D. Appl. Phys. 32 (1999) 726.

- [11] M.W. Cresswell, W.F. Guthrie, R.G. Dixon, R.A. Allen, C.E. Murabito, J.V.M. De Pinillos, J. Res. Natl. Inst. Stand. Technol. 111/3 (2006) 187.
- [12] R.A. Allen, B.A.A. Ende, M.W. Cresswell, C.E. Murabito, T.J. Headley, W.F. Guthrie, L.W. Linholm, C.H. Ellenwood, E.H. Bogardus, IEEE Trans. Semicond. Manuf. 16/2 (2003) 239.
- [13] B. Li, M.K. Kang, K. Lu, R. Huang, P.S. Ho, R.A. Allen, M.W. Cresswell, Nano Lett. 8/1 (2008) 92.
- [14] All the uncertainty ( $\pm$ ) presented in this work represents one standard deviation from the mean.
- [15] Certain equipment, instruments or materials are identified in this paper in order to adequately specify the experimental details. Such identification does not imply recommendation by the National Institute of Standards and Technology nor does it imply the materials are necessarily the best available for the purpose.